Tight Coordination of Protein Translation and HSF1 Activation Supports the Anabolic Malignant State

Sandro Santagata *et al.*

Science **341**, (2013);
DOI: 10.1126/science.1238303

Science (print ISSN 0036-8075; online ISSN 1095-9203) is published weekly, except the last week in December, by the American Association for the Advancement of Science, 1200 New York Avenue NW, Washington, DC 20005.

Tight Coordination of Protein Translation and HSF1 Activation Supports the Anabolic Malignant State

Sandro Santagata, Marc L. Mendillo, Yun-chi Tang, Aravind Subramanian, Casey C. Perley, Stéphane P. Roche, Bang Wong, Rajiv Narayan, Hyoungtae Kwon, Martina Koeva, Angelika Amon, Todd R. Golub, John A. Porco Jr., Luke Whitesell,* Susan Lindquist*

READ THE FULL ARTICLE ONLINE
http://dx.doi.org/10.1126/science.1238303

Cite this article as S. Santagata *et al.*, *Science* **341**, 1238303 (2013).
DOI: 10.1126/science.1238303

Introduction: Ribosome biogenesis is commonly up-regulated to satisfy the increased anabolic demands associated with malignant transformation and tumor growth. Many different oncogenic signaling pathways converge on the ribosome to increase translational flux. Despite the detailed understanding of ribosome regulation in cancer, it is not clear whether the net translational activity of the ribosome can itself regulate transcriptional programs that support and promote the malignant state.

Methods: To investigate the transcriptional effects of modulating translational activity in malignant cells, we used integrated chemical and genetic approaches, including a gene signature–based genetic and chemical screen of more than 600,000 gene expression profiles (LINCS database) and an independent, reporter-based chemical screen of more than 300,000 compounds. A lead compound was tested in several cell lines unified by their increased dependence on HSF1 activation for growth and survival, and in an in vivo cancer model.

Results: Inhibiting translation led to large changes in the transcriptome. The single most enriched category consisted of genes regulated by the heat-shock transcription factor, HSF1. The most down-regulated mRNA was *HSPA8*, which encodes the constitutive HSP70 chaperone that helps to fold nascent polypeptides. The expression of many other genes that HSF1 coordinates to support cancer was also strongly affected. HSF1 protein levels were unchanged, but HSF1 DNA occupancy was nearly eliminated. Inhibition of the HSF1-regulated gene expression program is thus a dominant transcriptional effect elicited by inhibiting protein translation.

Using a gene signature of HSF1 inactivation to query the LINCS database revealed a strong connection between HSF1 inactivation and perturbations that inhibit protein translation, including a broad spectrum of chemical and genetic interventions that target the ribosome, eukaryotic initiation factors (eIFs), aminoacyl tRNA synthetases, and upstream signaling/regulatory pathways that control translation.

Our high-throughput small-molecule screen identified rocaglamide A, an inhibitor of translation initiation, as the strongest inhibitor of HSF1 activation. An analog of this compound, RHT, increased thioredoxin-interacting protein (TXNIP) mRNA and protein levels and decreased glucose uptake and lactate production. Cell-based cancer models characterized by high dependence on HSF1 activation for growth and survival were highly sensitive to RHT, as were cells derived from diverse hematopoietic malignancies. RHT had a strong antitumor effect—with marked inhibition of HSF1 activity and glucose uptake—against xenografted acute myeloid leukemia cells.

Discussion: The ribosome functions as a central information hub in malignant cells: Translational flux conveys information about the cell's metabolic status to regulate the transcriptional programs that support it. Multiple unbiased chemical and genetic approaches establish HSF1 as a prime transducer of this information, centrally poised to regulate the transcription of genes that support protein folding, biomass expansion, anabolic metabolism, cellular proliferation, and survival. Targeting translation initiation may offer a strategy for reversing HSF1 activation, disabling metabolic and cytoprotective pathways in malignant cells.

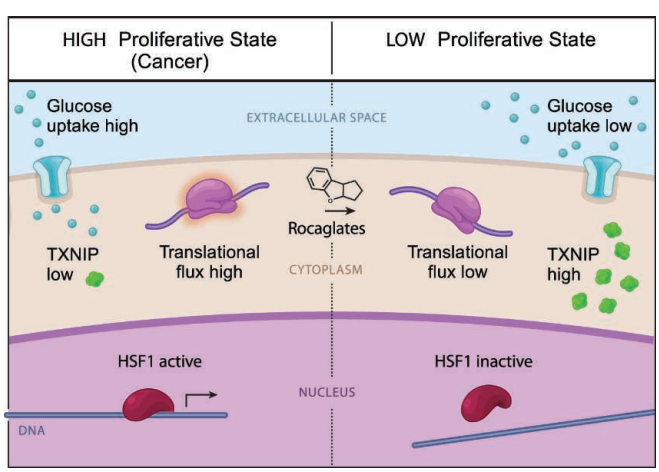

HSF1 at the crossroads of protein translation and metabolism. (**Left**) Cancers activate an HSF1-regulated transcriptional program to adapt to the anabolic demands of relentless biomass expansion. Glucose uptake increases, and expression of TXNIP, an inhibitor of glucose uptake, drops. (**Right**) Down-regulating translation with rocaglate scaffold initiation inhibitors reverses cancer-associated HSF1 activation. Glucose uptake drops as TXNIP levels rise.

FIGURES IN THE FULL ARTICLE

SUPPLEMENTARY MATERIALS

Materials and Methods
Figs. S1 to S9
Tables S1 to S5
References and Notes

RELATED ITEMS IN *SCIENCE*

V. Gandin, I. Topisirovic, Trans-HFS1 express. *Science* **341**, 242-243 (2013).
DOI: 10.1126/science.1242359

The list of author affiliations is available in the full article online.
*Corresponding author. E-mail: whitesell@wi.mit.edu (L.W.); lindquist_admin@wi.mit.edu (S.L.)

Tight Coordination of Protein Translation and HSF1 Activation Supports the Anabolic Malignant State

Sandro Santagata,[1,2,3]* Marc L. Mendillo,[3,4]* Yun-chi Tang,[4,5]† Aravind Subramanian,[6] Casey C. Perley,[3,4] Stéphane P. Roche,[7] Bang Wong,[6] Rajiv Narayan,[6] Hyoungtae Kwon,[3,4] Martina Koeva,[3,4] Angelika Amon,[4,5] Todd R. Golub,[6] John A. Porco Jr.,[7] Luke Whitesell,[3]‡ Susan Lindquist[3,4]‡

The ribosome is centrally situated to sense metabolic states, but whether its activity, in turn, coherently rewires transcriptional responses is unknown. Here, through integrated chemical-genetic analyses, we found that a dominant transcriptional effect of blocking protein translation in cancer cells was inactivation of heat shock factor 1 (HSF1), a multifaceted transcriptional regulator of the heat-shock response and many other cellular processes essential for anabolic metabolism, cellular proliferation, and tumorigenesis. These analyses linked translational flux to the regulation of HSF1 transcriptional activity and to the modulation of energy metabolism. Targeting this link with translation initiation inhibitors such as rocaglates deprived cancer cells of their energy and chaperone armamentarium and selectively impaired the proliferation of both malignant and premalignant cells with early-stage oncogenic lesions.

Regulation of ribosome activity is critical for supporting cellular proliferation. In cancer, ribosome biogenesis is commonly increased to satisfy the increased anabolic demands associated with malignant transformation and tumor growth (*1*–*4*). In addition, many different oncogenic signaling pathways converge on the ribosome to modulate its function (*5*, *6*). These inputs are integrated, and the net ribosomal translational activity is tuned to reflect the metabolic and proliferative state of the cell. Despite the detailed understanding of ribosome regulation in cancer, it is not well understood whether the net translational activity of the ribosome can itself be conveyed to regulate transcriptional programs that support and promote the malignant state. Is a coherent and coordinated transcriptional response triggered by modulating translation activity?

[1]Department of Pathology, Brigham and Women's Hospital (BWH), and Harvard Medical School, Boston, MA 02215, USA. [2]Dana Farber Cancer Institute, Boston, MA 02215, USA. [3]Whitehead Institute for Biomedical Research (WIBR), Cambridge, MA 02142, USA. [4]Howard Hughes Medical Institute, Department of Biology, Massachusetts Institute of Technology (MIT), Cambridge, MA 02142, USA. [5]David H. Koch Institute for Integrative Cancer Research and Howard Hughes Medical Institute, MIT, Cambridge, MA 02142, USA. [6]Broad Institute of MIT and Harvard, Cambridge, MA 02142, USA. [7]Department of Chemistry, Center for Chemical Methodology and Library Development (CMLD-BU), Boston University, Boston, MA 02215, USA.

*These authors contributed equally to this work.

†Present address: Institute of Health Sciences, Shanghai Institutes for Biological Sciences, Chinese Academy of Sciences & Shanghai Jiao Tong University School of Medicine, 20025 Shanghai, China.

‡Corresponding author. E-mail: whitesell@wi.mit.edu (L.W.); lindquist_admin@wi.mit.edu (S.L.)

Results

Inhibiting Translational Flux Inactivates HSF1

To investigate the transcriptional effects of reducing translational flux through the ribosome in malignant cells, we analyzed the mRNA expression profiles of breast cancer cells after treatment with various inhibitors of translation elongation (anisomycin, emetine, cephaeline, and cycloheximide). Large changes in the transcriptome were highly correlated across all four inhibitors [Pearson correlation coefficient (r) between 0.85 to 0.97 for all pairwise correlations]. The most strongly enriched category consisted of genes regulated by promoters that contain DNA binding motifs for the heat-shock transcription factor known as heat shock factor 1 (HSF1) ($P = 9.87 \times 10^{-7}$) (Fig. 1A and table S1). Of the 13,258 genes measured, the single most down-regulated mRNA was *HSPA8*, which encodes a constitutive HSP70 chaperone that folds nascent polypeptides as they emerge from the ribosome (Fig. 1B and table S2) (*7*). *HSPA1A*, a cancer-induced *HSP70* gene, was also among the 10 most down-regulated mRNAs. This transcriptional response suggested that reduced translational flux causes a profound shift in the activity of HSF1.

In a wide range of cancers, HSF1 regulates a transcriptional network that is distinct from the conventional network activated by thermal stress (*8*). This cancer network includes many classic "heat-shock" genes. But, it also includes a broad cadre of other genes that play critical roles in malignancy, some of which are positively regulated by HSF1 and some negatively regulated. All four inhibitors of translation elongation affected genes in the HSF1 cancer network ($P = 0.016$) (Fig. 1C and fig. S1). Genes that are positively regulated by HSF1 were down-regulated when translational flux through the ribosome was reduced. These genes included drivers of cell proliferation and mitogenic signaling (such as *CENPA*, *CKS1B*, and *PRKCA*), transcription and mRNA processing (such as *LSM2* and *LSM4*), protein synthesis (such as *FXR1* and *MRPL18*), energy metabolism (such as *MAT2A*, *SLC5A3*, *PGK1*, *MBOAT7*, and *SPR*), and invasion/metastasis (such as *EMP2* and *LTBP1*). In a complementary fashion, genes that are negatively regulated by HSF1 were up-regulated when translational flux through the ribosome was reduced. These included genes that promote differentiation (such as *NOTCH2NL*), cellular adhesion (such as *EFEMP1* and *LAMA5*), and apoptosis (such as *BCL10*, *CFLAR*, and *SPTAN1*).

This effect of translation inhibition on HSF1-regulated transcription led us to examine the genome-wide pattern of DNA occupancy by HSF1 in breast cancer cells. After a 6-hour exposure to cycloheximide, we performed chromatin immunoprecipitation coupled with massively parallel DNA sequencing (ChIP-Seq) using a previously validated antibody against HSF1 (*8*). Despite cycloheximide treatment, HSF1 protein levels themselves remained unchanged (Fig. 1D). In contrast to DNA occupancy by RNA-polymerase II (which was not globally reduced), HSF1 occupancy was nearly eliminated (Fig. 1, E to G, fig. S2, and table S3). This held true for genes that were either positively or negatively regulated by HSF1, as well as for genes shared with the classic heat-shock response and genes specific to the HSF1 cancer program (table S3). Together, these data pointed to a link between the activity of the ribosome and the activity of HSF1.

LINCS Establishes Translation as a Potent Regulator of HSF1 in Cancer Cells

To further investigate the link between the HSF1 activity and translational program, we turned to an expression-profiling resource created by the Library of Integrated Network-based Cellular Signatures (LINCS) program (Fig. 2 and supplementary materials, materials and methods). The LINCS database is a large catalog of gene-expression profiles collected from human cells treated with chemical (small-molecule) and genetic [short hairpin RNA (shRNA)] perturbations.

We generated a query signature for HSF1 inactivation from expression profiles of breast cancer cells that had been treated with HSF1 shRNAs (supplementary materials, materials and methods) (*8*). This signature included both genes that were up-regulated by HSF1 inactivation and down-regulated by HSF1 inactivation. We compared our HSF1 query signature with LINCS expression profiles from nine cell lines that are currently the most extensively characterized in this database (Fig. 2A). Eight of these are cancer lines of diverse histopathologic origin. These lines have been treated individually with 3866 small-molecule compounds or 16,665 shRNAs targeting 4219 genes. The compounds used for these gene expression

profiles encompassed U.S. Food and Drug Administration (FDA)–approved drugs and known bioactives. The shRNAs used were directed against the known targets of these compounds, against genes in related pathways, or against other genes that have been implicated in a variety of human diseases. In all, we compared our HSF1 signature with 161,636 LINCS signatures, each generated from at least three replicates (for a total of 614,216 profiles.)

As expected, the LINCS perturbations that negatively correlated with our HSF1 inactivation signature were enriched for known activators of HSF1. They included shRNAs that target components of the proteasome. They also included compounds that inhibit the proteasome and that inhibit HSP90 (Fig. 2, B and C and table S4).

The LINCS perturbations that positively correlated with our HSF1 inactivation signature were most highly enriched for translation inhibitors (cephaeline, cycloheximide, and emetine) (Fig. 2, B and C, and table S4). These perturbations were also highly enriched for compounds that target signaling pathways that regulate protein translation: phosphatidylinositol 3-kinase (PI3Kinase)/mammalian target of rapamycin (mTOR) inhibitors (Fig. 2B and table S4). Of the nearly 200 gene ontology classes analyzed, the ribosome subunit family was the single most enriched (Fig. 2, B and C, and table S4). In addition, eukaryotic initiation factors (eIFs) and aminoacyl tRNA synthetases were also highly enriched. This unbiased analysis using the LINCS database demonstrates the connection between translational flux and the function of HSF1 in cancer.

An Unbiased High-Throughput Chemical Screen for HSF1 Inhibitors

To find alternate ways to inhibit HSF1, we performed a large high-throughput chemical screen. We screened 301,024 compounds through the U.S. National Institutes of Health (NIH) Molecular Libraries Probe Center Network (MLPCN; Pubchem AID, 2118) (Fig. 3A) using an HSF1-regulated reporter driven by consensus heat-shock elements (HSEs). To accommodate constraints of the high-throughput 384-well format (supplementary materials, materials and methods), we used a reporter cell line stably transduced with a luminescence-based reporter and induced HSF1 activation with a simple proteotoxic stressor (the proteasome inhibitor MG132).

Approximately 2500 hit compounds from the primary screen, which blocked induction of the reporter, were then counter-screened with an independent dual reporter cell line (Fig. 3B) so as to eliminate nonselective inhibitors. This second line had been stably transduced with two constructs, one encoding a green fluorescent protein (GFP) driven by HSEs and the other encoding a red fluorescent protein (RFP) driven by a doxycycline-regulated control promoter. Compounds that selectively inhibit HSF1 activity should suppress GFP expression in this cell line but should not suppress doxycycline-mediated induction of RFP. Notably, compounds that are thought to selectively inhibit HSF1—such as triptolide, quercetin, KNK423, and KNK437 (*9*)—all suppressed both reporters (fig. S3). Thus, these compounds

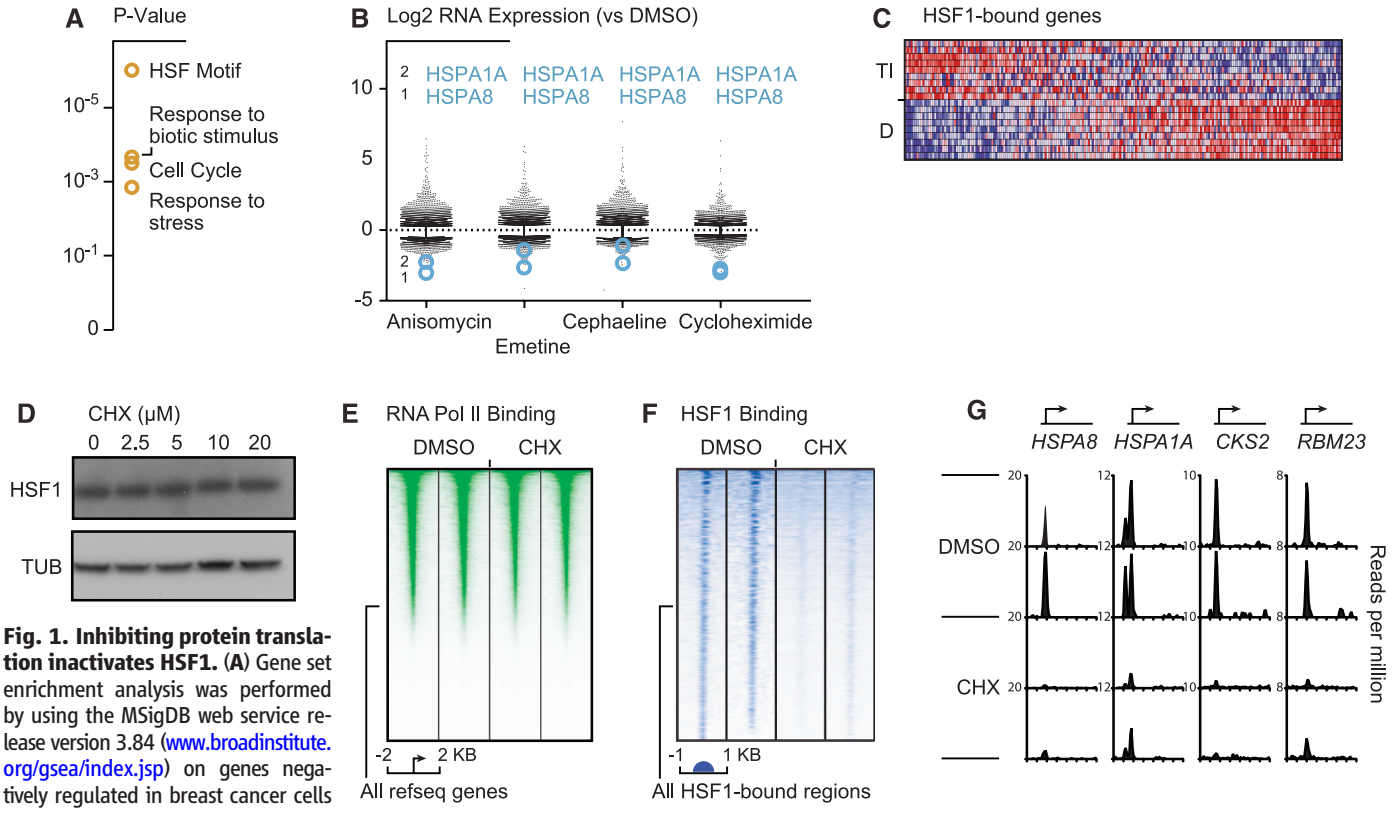

Fig. 1. Inhibiting protein translation inactivates HSF1. (**A**) Gene set enrichment analysis was performed by using the MSigDB web service release version 3.84 (www.broadinstitute.org/gsea/index.jsp) on genes negatively regulated in breast cancer cells following a 6-hour incubation with inhibitors of protein translation elongation. Selected results are displayed; complete GSEA results are provided in table S1. (**B**) Scatter plot of levels of mRNA transcripts (log2) after a 6-hour incubation with the indicated inhibitors of protein translation elongation versus control dimethyl sulfoxide (DMSO). The levels of HSPA1A and HSPA8 are indicated for each elongation inhibitor. (**C**) Translation elongation inhibitors alter the basal transcriptional program of HSF1 in breast cancer cells. Genes bound by HSF1 in MCF7 were ranked by their differential expression between cells treated with translation elongation inhibitors (TI) and control DMSO (D). Each column represents a gene and is normalized across the column, with high expression in red and low expression in blue. (**D**) An immunoblot shows the levels of HSF1 protein and the loading control tubulin after a 6-hour exposure to the indicated concentrations of cycloheximide (CHX). (**E**) Heat map of RNA polymerase II ChIP-Seq read density in MCF7 cells that were treated with DMSO or 10 μM CHX for 6 hours. Genomic regions from −2 kb to +2 kb relative to the transcription start site for all RefSeq genes are shown. (**F**) Heat map of HSF1 ChIP-Seq read density in MCF7 cells that were treated with DMSO or 10 μM CHX for 6 hours. Genomic regions from −1 kb to +1 kb relative to the peak of HSF1 binding for all HSF1-enriched regions (union of all HSF1-enriched regions in the four data sets depicted here) are shown. (**G**) Representative genes bound by HSF1 in MCF7 cells (*HSPA8*, *HSPA1A*, *CKS2*, and *RBM23*). The *x* axis depicts from −2kb from the transcription start site (TSS) to 5 kb from the TSS for each gene.

are far less specific for HSF1 than commonly assumed.

More to the point, the chemical screen results also suggested a link between HSF1 activation and the translation machinery. By far the most potent and selective hit to emerge from the 301,024 compounds we tested was the rocaglate known as rocaglamide A [median inhibitory concentration (IC_{50}) of ~50 nM for the heat shock reporter versus IC_{50} >1000 nM for the control reporter] (Fig. 3C). This natural product inhibits the function of the translation initiation factor eIF4A, a DEAD box RNA helicase (*10*, *11*). Presumably, it passed counterscreening in our secondary assay with the dual reporter system because translation of the doxycycline-regulated RFP control does not require the classical cap-dependent initiation complex.

To define structure-activity relationships for inhibition of the HSE reporter by rocaglamide A, we used our dual reporter system to test 38 additional rocaglates (fig. S4). These included both natural products and totally synthetic analogs prepared with photocycloaddition methods (*12*, *13*). Five hydroxamate analogs were more potent than rocaglamide A at inhibiting the HSE reporter while retaining similar selectivity (table S5). The most potent inhibitor had an IC_{50} of ~20 nM (table S5). We named this compound [previously reported as "8e" (*13*)] Rohinitib (or RHT), for Rocaglate Heat Shock, Initiation of Translation Inhibitor.

Characterizing the Effects of RHT on Cancer Cells

To validate findings from our engineered reporter system, we measured the effects of RHT on the basal expression of several endogenous HSF1-regulated transcripts (Fig. 3D and figs. S5 and S6). RHT did not reduce the transcript levels of the control housekeeping genes *B2M* and *GAPDH*. Nor did it reduce the transcript levels of *HSF1* itself (Fig. 3D and fig. S6A). However, mRNA levels of Hsp40 (*DNAJA1*) and Hsp70 genes (*HSPA1B* and *HSPA8*) dropped substantially. The most dramatically affected was the constitutively expressed *HSPA8* gene (>90% reduction) (Fig. 3D). This was also the gene that we had found to be the most strongly repressed by translation elongation inhibitors (Fig. 1B).

The effects of RHT were not due to reductions in HSF1 protein levels, which remained constant (Fig. 3E and fig. S6B). The sharp decrease in *HSP70* mRNA levels in response to RHT held true across a histologically diverse panel of human cancer cell lines (MCF7, breast adenocarcinoma; MO91, myeloid leukemia; CHP100, sarcoma; and HeLa, cervical carcinoma) as well as in artificially transformed 293T kidney cells (Fig. 3D and fig. S6, A and C). RHT had a much smaller effect on *HSP70* mRNA levels in proliferating but nontumorigenic diploid cells (WI38 and IMR90) (fig. S6C).

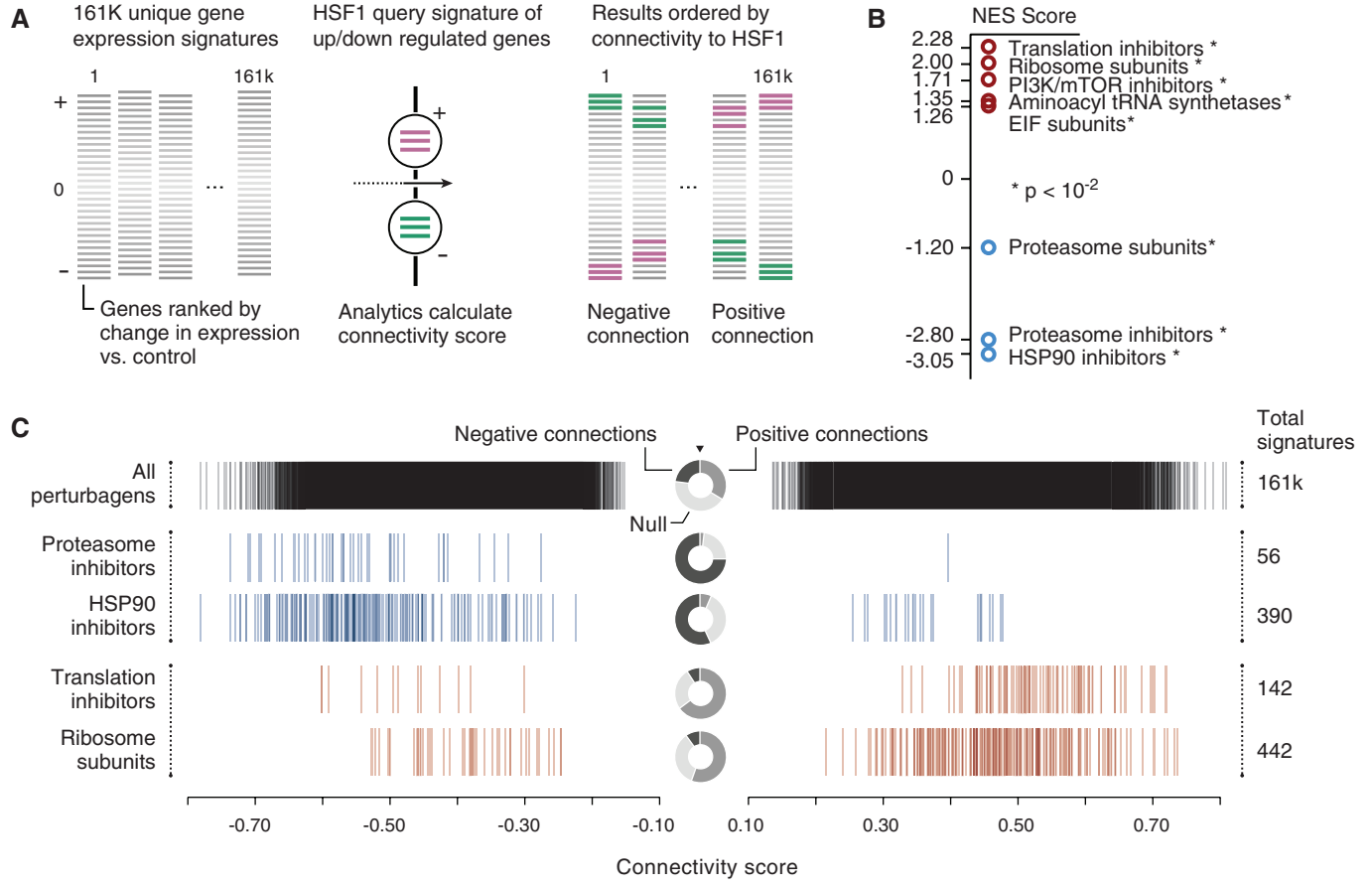

Fig. 2. LINCS analysis reveals that targeting protein translation inactivates HSF1. (**A**) Schematic representation of the LINCS analysis used to identify chemical and genetic modulators that are correlated with HSF1 inactivation (supplementary materials, materials and methods). Pink represents genes whose levels increase, and green represents genes whose levels decrease, after shRNA-mediated knockdown of HSF1. (**B**) GSEA results of our HSF1 inactivation signature LINCS analysis. Perturbation signatures were rank-ordered by connectivity with the HSF1 inactivation signature, and enrichment was determined for KEGG pathway gene sets and ATC chemical classes (details are available in the supplementary materials, materials and methods). Normalized enrichment score (NES) of selected results are plotted (complete GSEA results are provided in table S4). (**C**) Barcode plot of the connectivity score of all of the individual perturbations comprising the indicated enriched chemical or gene sets. The bagel plot in the center of the barcode plot summarizes the positive, negative, and null (not connected) fractions for the indicated enriched class. All perturbations that are positively or negatively connected for the indicated enriched classes are shown. Total perturbations in each class are indicated on the right of the plot. Blue represents negatively connected, and red represents positively connected, classes of enriched perturbations.

To obtain a more direct and global view of RHT's effects on HSF1 activity, we examined genome-wide promoter occupancy by means of ChIP-Seq analysis. RHT virtually abolished HSF1 binding throughout the genome (Fig. 4, A and B; fig. S6D; and table S3). As had occurred with cycloheximide, RHT affected both genes that are positively regulated by HSF1 and genes that are negatively regulated by HSF1 (Fig. 4A). Furthermore, it affected both classic heat-shock genes and genes specific to the HSF1 cancer program (table S3). The effects on HSF1 DNA occupancy occurred at concentrations of cycloheximide and RHT that inhibit the ribosome activity to a similar extent (Fig. 4C).

Rocaglates Modulate Tumor Energy Metabolism

While characterizing the effects of RHT on the transcriptome, we noted that treated cells failed to acidify the culture medium (detected incidentally by the color of the pH indicator phenol red included in standard media). This suggested a reversal of the "Warburg effect," a metabolic shift responsible for increased lactic acid production by many cancers. Genetic compromise of HSF1 drives a shift in metabolism in both cell culture and animal models (*14*, *15*). Hence, this effect of RHT is consistent with inactivation of HSF1.

Our mRNA expression profiling of rocaglate-treated breast cancer cells also revealed that mRNA levels for thioredoxin-interacting protein (TXNIP) were up-regulated. TXNIP is a powerful negative regulator of glucose uptake and is a well-established regulator of cellular energy status (*16*, *17*). Its expression is dramatically reduced in malignant cells, leading to increased glucose uptake (*18*). Conversely, increasing TXNIP levels leads to reduced glucose uptake (*16*). The induction of TXNIP mRNA by RHT was observed across a diverse panel of tumor cell lines (Fig. 5A). TXNIP protein levels also increased sharply despite a marked reduction in the levels of other short-lived proteins, such as p53 (Fig. 5B). Although we did not detect HSF1 bound to the TXNIP locus, HSF1 null cells showed higher levels of TXNIP (fig. S7). In addition, HSF1 did directly regulate a group of other genes involved in energy metabolism (including *MAT2A*, *SLC5A3*, and *PGK1*). At a functional level, the effects of RHT were associated with concentration-dependent reductions in both glucose uptake and lactate production (Fig. 5C). Thus, the effects of RHT on protein translation, HSF1 activation, and energy metabolism—processes lying at the core of the anabolic state of cancer—appear to be coordinated.

Rocaglates Selectively Target Pre-Malignant Cells with Early-Stage Oncogenic Lesions

Does this tight coordination create vulnerabilities for the malignant phenotype that could be exploited as a therapeutic strategy? We looked at a range of cell-based cancer models unified by their increased dependence on HSF1 activation for growth and survival. Although it occurs very early during oncogenesis, simple loss of the tumor suppressor *Nf1* leads to an increase in HSF1 protein levels, nuclear localization, and transcriptional activation (*19*). We treated mouse embryonic fibroblasts (MEFs) in which *Nf1* was knocked out and wild-type littermate control MEFs in which HSF1 was not activated, with either RHT or with cycloheximide. The two cell types were similarly sensitive to cycloheximide. However, *Nf1*-null MEFs were more sensitive than were wild-type MEFs to RHT (Fig. 6A). In this model for an early event in tumorigenesis, targeting translation initiation rather than translation elongation seems to provide a more selective, better tolerated approach for disrupting the link between translation and HSF1 activation.

A second engineered system allowed us to ask whether rocaglates would selectively inhibit the growth of cells carrying a simple chromosomal aberration that models another common early event in the development of cancer: aneuploidy. Chromosomal imbalances lead to both increased energy and proteotoxic stress. This is reflected by the elevation of the HSF1-regulated chaperone protein HSP72, encoded by *HSPA1A* (*20*). We isolated MEFs from mice carrying Robertsonian fusions for chromosome 13 (*21*). These MEFs (TS13) carry a single extra copy of 120 Mb of chromosome 13, introducing an additional copy of 843 genes.

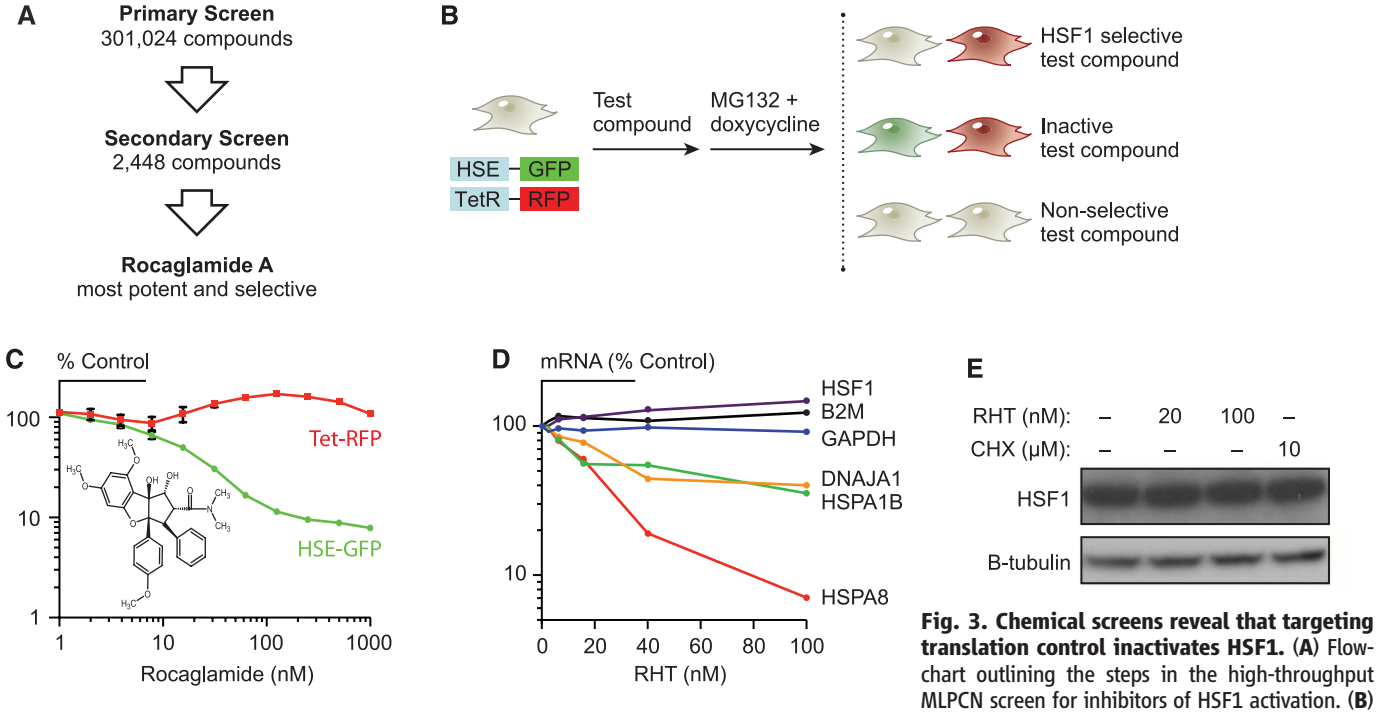

Fig. 3. Chemical screens reveal that targeting translation control inactivates HSF1. (**A**) Flowchart outlining the steps in the high-throughput MLPCN screen for inhibitors of HSF1 activation. (**B**) Schematic of dual-reporter cell line used to counter-screen primary screen hits. GFP expression is regulated by a heat shock–inducible promoter. RFP expression is regulated by a doxycycline response element (TetR). (**C**) Effect of rocaglamide A on the HSE-driven GFP and doxycycline-driven RFP signals after incubation with 2.5 mM MG132 and 2 μg/ml doxycycline. Chemical structure of rocaglamide A is displayed in the inset. Error bars indicate mean ± SEM of quadruplicates. (**D**) Effect of RHT on HSF1-regulated and control endogenous mRNA transcript levels in M0-91 leukemia cells measured by means of nanostring nCounter after a 6-hour incubation with indicated concentrations of RHT. Levels of endogenous transcript are shown as percent of DMSO-treated control. Mean of duplicates are reported. (**E**) HSF1 protein levels are not affected in M0-91 leukemia cells treated with RHT. Immunoblot shows the levels of HSF1 protein and the loading control (Tubulin) after a 6-hour exposure to the indicated concentrations of RHT.

Cycloheximide, as well as conventional cytotoxic chemotherapeutics (taxol and hydroxyurea), inhibited the growth of both trisomic and littermate control MEFs to an equal extent (Fig. 6B and fig. S8). But, trisomic MEFs ($P < 0.0001$) were more sensitive than wild-type MEFs to RHT (Fig. 6B). Thus, again in this model for an early neoplastic change that activates HSF1, targeting translation initiation seems to provide a better tolerated, more selective approach for targeting the malignant state.

HSF1 activation is even more prominent in advanced malignancies (*8*, *22*, *23*). For example, colon cancers frequently show immunohistochemical evidence of strong HSF1 activation (Fig. 6C) and this correlates with poor clinical outcome (*8*). We mined publicly available expression profiling from colon cancer lines with highly aneuploid karyotypes [chromosomal instability (CIN)] and from colon cancer lines with near-euploid karyotypes but microsatellite instability (MIN). The CIN lines expressed markedly higher levels of *HSPA1A*, which is consistent with greater levels of proteotoxic stress and greater activation of the HSF1-regulated cancer program (Fig. 6, D and E). Next, we tested several patient-derived colon cancer lines with CIN and several patient-derived colon cancer lines with MIN for sensitivity to inhibition by RHT. The CIN lines were much more sensitive than were the MIN lines. Nontransformed colon epithelial cell lines with euploid chromosome content were the least sensitive of all the lines we tested (Fig. 6F).

Rocaglates Suppress the Growth of Cancer Cells and Tumors

Some rocaglates have previously been shown to exert profound anticancer activity (*10*, *24*–*26*). We tested RHT against a collection of cell lines including nontransformed diploid lines and cancer cell lines with diverse histopathological origins and oncogenic lesions (Fig. 7A). The nontransformed cell lines were relatively resistant to RHT (IC_{50} from 100 to 300 nM). All cancer cell lines were sensitive to RHT ($IC_{50} < 30$ nM); the hematopoietic tumor cell lines were especially sensitive ($IC_{50} \leq 6$ nM). We used one of these hematopoietic tumor lines, the M0-91 cell line originally derived from a patient with acute myeloid leukemia (*27*), to further characterize the effects of RHT. RHT strongly suppressed *HSPA8* mRNA levels in M0-91 cells and induced *TXNIP* mRNA (Fig. 7B). In addition, RHT sharply decreased glucose uptake by these cells (Fig. 7C).

Are the effects of RHT in cell culture achievable at drug exposures that are systemically tolerable in animals? To directly address this critical issue of therapeutic index, we first used standard in vitro assays to test whether RHT had sufficiently drug-like properties to justify testing in mice (fig. S9). We assessed aqueous solubility, plasma stability, plasma protein binding, hepatic microsome stability, and cellular permeability (fig. S9A). No severe liabilities were found. We next established minimally toxic parameters for dosing mice with RHT and performed a plasma pharmacokinetic study after administration of 1 mg/kg subcutaneously (fig. S9, B and C). Peak plasma levels were far in excess of those required for the key biological activities we had demonstrated in cell culture. Moreover, levels required for anticancer activity in vitro were maintained in excess of 2 hours in vivo.

We next established subcutaneous tumor xenografts of the human myeloid leukemia cell line M091 in nonobese diabetic (NOD)–severe combined immunodeficient (SCID) immunocompromised mice. When the mean tumor volume reached 100 mm^3, we administered RHT at 1 mg/kg for 4 consecutive days each week for 3 weeks (Fig. 7D). Over the treatment period, there was no evidence of gross systemic toxicity (fig. S9D). RHT mediated marked, sustained inhibition of the growth of this very aggressive myeloid malignancy (Fig. 7D).

We then pursued pharmacodynamics studies. Mice bearing xenografts were given a single dose of RHT. Tumors were explanted 4 hours later, and *HSPA8* and *TXNIP* mRNA levels were determined by means of reverse transcription polymerase chain reaction (RT-PCR) (Fig. 7E). Similar to

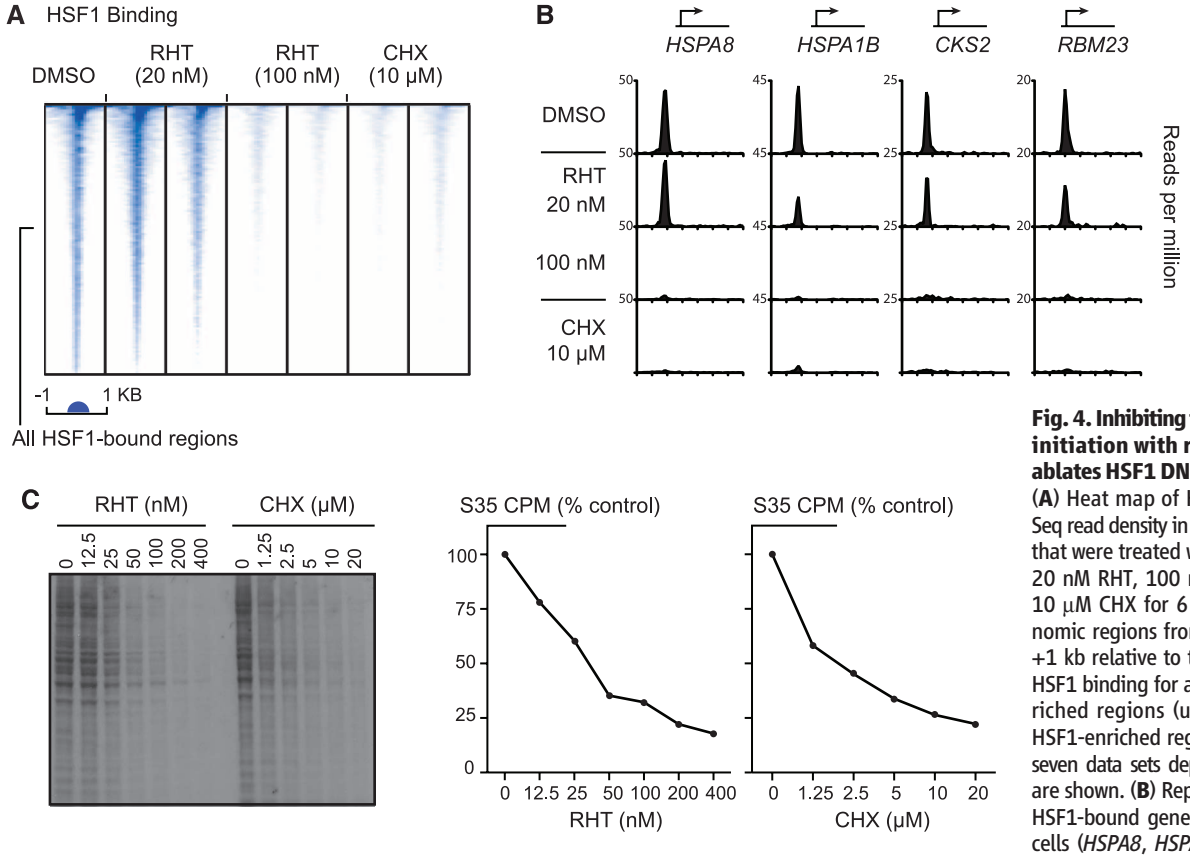

Fig. 4. Inhibiting translation initiation with rocaglates ablates HSF1 DNA binding. (**A**) Heat map of HSF1 ChIP-Seq read density in M0-91 cells that were treated with DMSO, 20 nM RHT, 100 nM RHT, or 10 μM CHX for 6 hours. Genomic regions from −1 kb to +1 kb relative to the peak of HSF1 binding for all HSF1 enriched regions (union of all HSF1-enriched regions in the seven data sets depicted here) are shown. (**B**) Representative HSF1-bound genes in M0-91 cells (*HSPA8*, *HSPA1B*, *CKS2*, and *RBM23*). The *x* axis depicts from −2 kb from the transcription start site (TSS) to 5 kb from the TSS for each gene. (**C**) Autoradiograph of S35-labeled protein lysates from MCF7 cells treated for 6 hours with the indicated concentrations of RHT or CHX. Graphs show the counts per minute from acetone precipitation of proteins in each sample, quantitated by using a scintillation counter.

the effects we observed in cell culture, RHT caused a strong decrease in *HSPA8* transcript levels and a strong increase in *TXNIP* transcript levels. In a separate experiment, we monitored the uptake of fluorescently labeled 2-deoxyglucose 48 hours after RHT dosing. RHT strongly suppressed uptake of this glucose analog by these tumors (Fig. 7F). Clearly, the effects of RHT achieved in cell culture could also be achieved in whole animals.

Discussion

HSF1 provides essential support for the malignant state by blocking apoptotic responses and promoting protein synthesis, anabolic energy metabolism, mitogenic signaling pathways, and pathways that facilitate invasion and metastasis (*8*, *14*, *15*, *19*, *23*, *28*–*30*). Here, we show that the ability of HSF1 to maintain this cancer program is exquisitely sensitive to translational activity.

Our work establishes that the ribosome could function as a central information hub: Translational flux conveys information about the cell's metabolic status to regulate the transcriptional programs that support it. The specific molecular mechanisms are likely to be multifaceted, but HSF1 is clearly a linchpin in this process. One plausible mechanism for the effects of translation inhibitors on HSF1 activity could involve the translation of mRNA for a modifier of HSF1 transcriptional activity that is sensitive to subtle changes in translation activity, involving eIF4A and/or other initiation factors. Because HSF1 regulates the expression of genes encoding for ribosomal subunits and other regulators of translation (*8*, *15*, *31*), the existence of a feedforward regulatory circuit involving the protein translation machinery and HSF1 is also possible.

HSF1 is centrally poised to support protein folding and biomass expansion as well as many other functions to which malignant cells are addicted (*8*, *14*, *15*, *32*). We postulate that the translation/HSF1 link we have uncovered in cancer may derive from ancient systems geared to align and synchronize essential cellular functions for growth and survival. In comparison, in the nematode HSF1 is a longevity factor, and in yeast it is an essential gene that participates in cotranslational quality control (*33*–*35*).

In man, the translation/HSF1 link is particularly important in supporting the malignant phenotype because it can respond to varied metabolic inputs that are commonly dysregulated in cancer (*5*, *6*, *36*–*38*). This translation/HSF1 link allows these metabolic inputs to bolster the cytoprotective milieu, helping tumor cells to accommodate the drastic internal imbalances arising during oncogenesis as well as the severe external stresses arising from therapeutic interventions (*39*). The tight coordination of protein translation and HSF1 activation, together with the many ways that cells integrate the derangements of malignancy with translational activity, suggests that unifying principles drive HSF1 activation across the extraordinarily wide range of human cancers in which that activation occurs (*8*, *22*).

Although cancer cells often co-opt powerful, adaptive nononcogene systems for their benefit (*40*), it now appears that by co-opting the link between the ribosome and HSF1, cancers become especially vulnerable to agents that target translation and its upstream regulatory pathways. In this regard, our animal experiments suggest that targeting translation initiation may offer a strategy for reversing HSF1 activation and disabling the metabolic and cytoprotective addictions of malignant cells.

Materials and Methods

Cell Lines

WI38, CHP100, HeLa, 293T, PC3, MCF7, and NIH3T3 cells were purchased from American Type Culture Collection (ATCC). Immortalized *Nf1* knockout MEFs and littermate wild-type control MEFs were kind gifts from K. Cichowski. Littermate-derived euploid and trisomic primary MEFs were described previously (*20*). RHT treatments experiments were performed by using chromosome 13 trisomic cell lines and littermate control euploid cell lines that carried a single Robertsonian translocation. Early-passage MEFs were used to ensure that additional karyotypic changes had not yet occurred. Two primary human cell lines (CCD112 CoN and CCD841 CoN), five MIN lines (HCT-116, HCT-15, DLD-1, SW48, and LoVo), and five CIN lines (Caco2, HT-29, SW403, SW480, and SW620) were obtained from ATCC. Chromosome number and karyotype information were obtained from the National Cancer Institute database and the COSMIC data set at the Sanger Institute. M0-91 cells were previously described (*27*). The M0-91 cell line used in this study were established from explanted M0-91 tumors that had been xenografted once in mice. All cell cultures were maintained under 5% CO_2 in media according to their specifications.

mRNA Expression Profiling and Analysis

Expression profiles for MCF7 cells treated for 6 hours with anisomycin (15 μM), emetine (7 μM), cephaeline (6 μM), and cycloheximide (14 μM) were previously deposited in the Connectivity Map (*41*). MCF7 cells were treated with 200 nM rocaglamide A or 50 nM RHT for 6 hours, and RNA was then purified after extraction with TRIzol reagent [Invitrogen (Carlsbad, CA), catalog no. 15596-026]. Gene expression analysis was

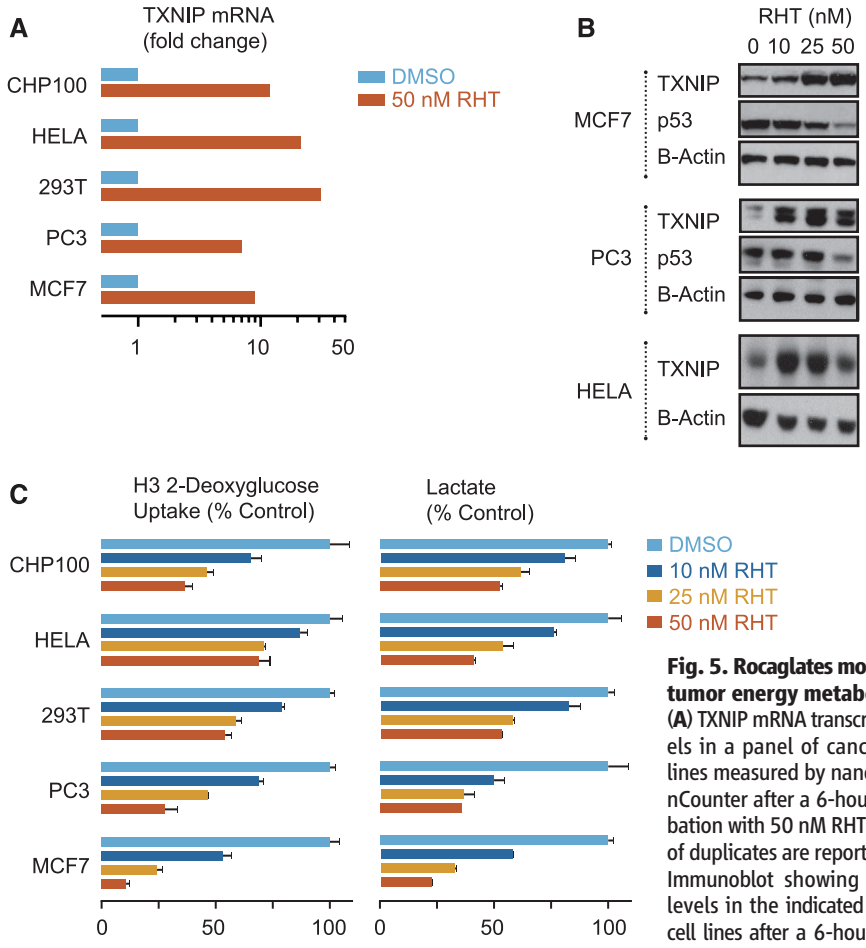

Fig. 5. Rocaglates modulate tumor energy metabolism. (**A**) TXNIP mRNA transcript levels in a panel of cancer cell lines measured by nanostring nCounter after a 6-hour incubation with 50 nM RHT. Mean of duplicates are reported. (**B**) Immunoblot showing TXNIP levels in the indicated cancer cell lines after a 6-hour incubation with the indicated concentration of RHT. β-actin is the loading control. The effect on p53, a short half-life protein, is shown. (**C**) Effects of the indicated amount of RHT on [H3]-2-deoxyglucose uptake (left) and lactate production (right) in a panel of cancer cell lines after 8 hours of incubation. Error bars indicate mean ± SEM of triplicates.

performed by using Affymetrix (Santa Clara, CA) GeneChip HT Human Genome U133A 96-Array Plates, and data was analyzed as previously described (*8*). All microarray raw data were deposited in a public database [National Center for Biotechnology Information Gene Expression Omnibus (GEO) pending]. Gene set enrichment analysis of the differentially expressed genes after treatment of MCF7 cells with translation elongation inhibitors was performed by using the gene set enrichment analysis (GSEA) Web site release version 3.84 (*42*). Enrichment for

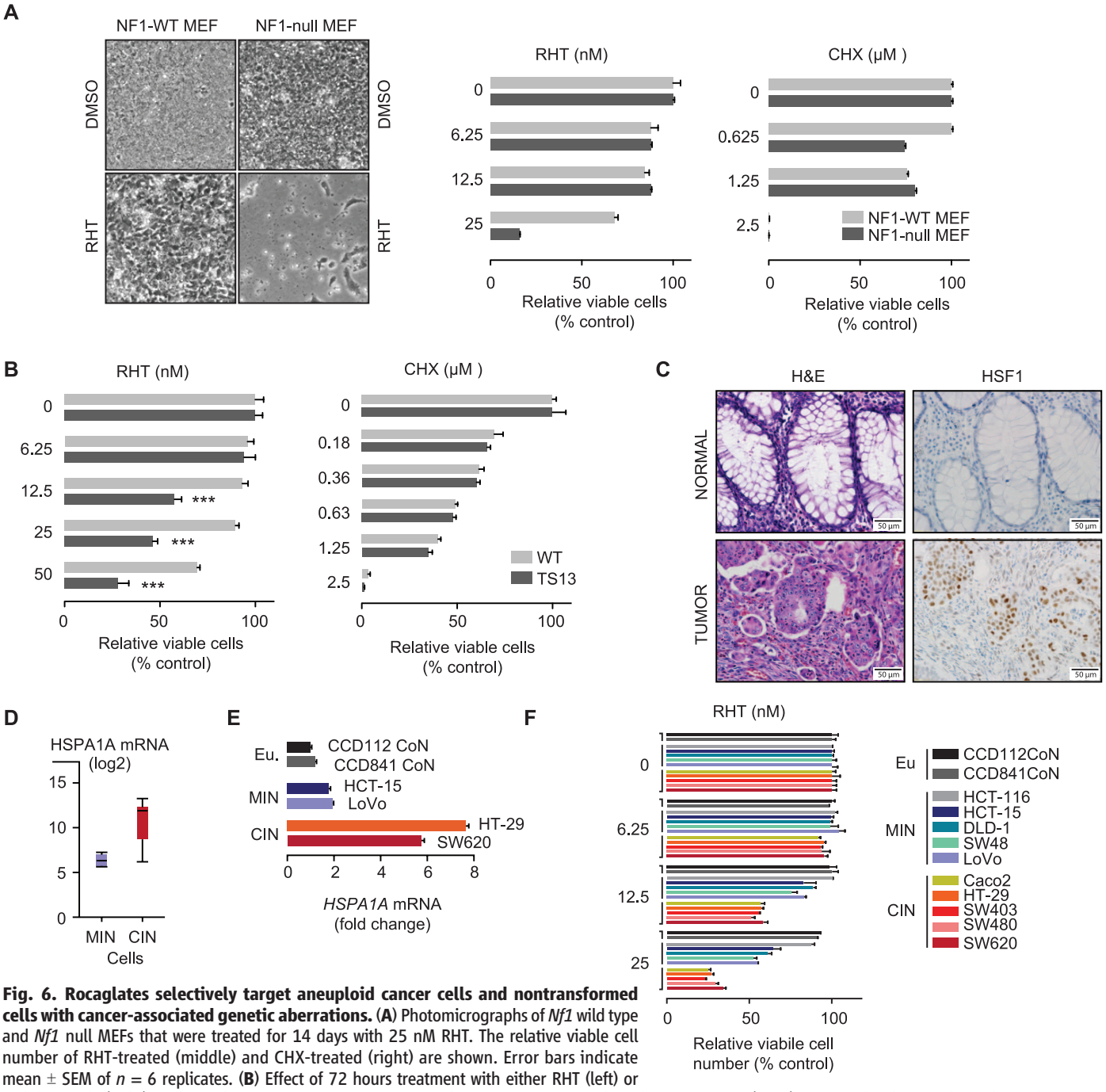

Fig. 6. Rocaglates selectively target aneuploid cancer cells and nontransformed cells with cancer-associated genetic aberrations. (**A**) Photomicrographs of *Nf1* wild type and *Nf1* null MEFs that were treated for 14 days with 25 nM RHT. The relative viable cell number of RHT-treated (middle) and CHX-treated (right) are shown. Error bars indicate mean ± SEM of $n = 6$ replicates. (**B**) Effect of 72 hours treatment with either RHT (left) or cycloheximide (right) on the proliferation of MEFs carrying a single extra copy of 120 Mb of chromosome 13 (TS13) compared with MEFs derived from littermate controls (WT), [mean ± SD, $n = 3$ replicates, ***$P < 0.001$, two-way analysis of variance (ANOVA)]. (**C**) Photomicrographs of normal colon epithelial cells and invasive colon adenocarcinoma (hematoxylin and eosin stains and HSF1 immunohistochemistry) from the same section of a human tumor resection (immunostained simultaneously). HSF1-expressing cells stain brown, and HSF1-negative cells stain blue from the toluidine blue counterstain. Scale bar, 50 μm. (**D**) *HSPA1A* mRNA transcript levels are elevated in colorectal adenocarcinomas with high-grade aneuploid karyotypes. Data from three MIN and nine CIN colon cancer cell lines from the GSK Cancer Cell Line Genomic Profiling Data as described in the methods. Box plot, bar is median, and whiskers are min and max (three cell lines in MIN category in triplicate 9 cell lines in CIN category in triplicate). (**E**) RT-PCR analysis of *HSPA1A* mRNA levels in the indicated euploid nontransformed cell lines, and MIN and CIN cancer cell lines. Error bars indicate mean ± SD of triplicates. (**F**) Effect of RHT on the proliferation of a panel of cell lines with high-grade aneuploid karyotypes (CIN lines: Caco2, HT29, SW403, SW480, and SW620); near-euploid karyotypes with microsatellite instability (MIN lines: HCT-116, HCT-15, DLD-1, SW48, and LoVo); or nontransformed colon epithelial cell lines with a euploid chromosomal number (CCD112CoN and CCD841CoN), (mean ± SD, $n = 3$ replicates, ***$P < 0.001$, two-way ANOVA) treated for 72 hours.

HSF1-bound genes among the genes differentially expressed after treatment of MCF7 cells with translation elongation inhibitors was conducted by using GSEA v2.08 software (*42*). HSF1-bound genes in MCF7 cells were defined as those genes bound in at least two of the four data sets [two data sets from this study and two from (*8*)].

Evaluation of *HSPA1A* mRNA levels was performed by using data from the GlaxoSmithKline (GSK) Cancer Cell Line Genomic Profiling Data https://cabig.nci.nih.gov/community/caArray_GSK-data. MIN lines used were HCT15, LS174T, SW48. CIN lines used were NCIH508, NCIH747, SW1116, SW1417, SW403, SW480, SW620, T84, and SW948.

ChiP-Seq and ChIP-PCR

Described in supplementary materials, materials and methods.

Immunoblot

Described in supplementary materials, materials and methods.

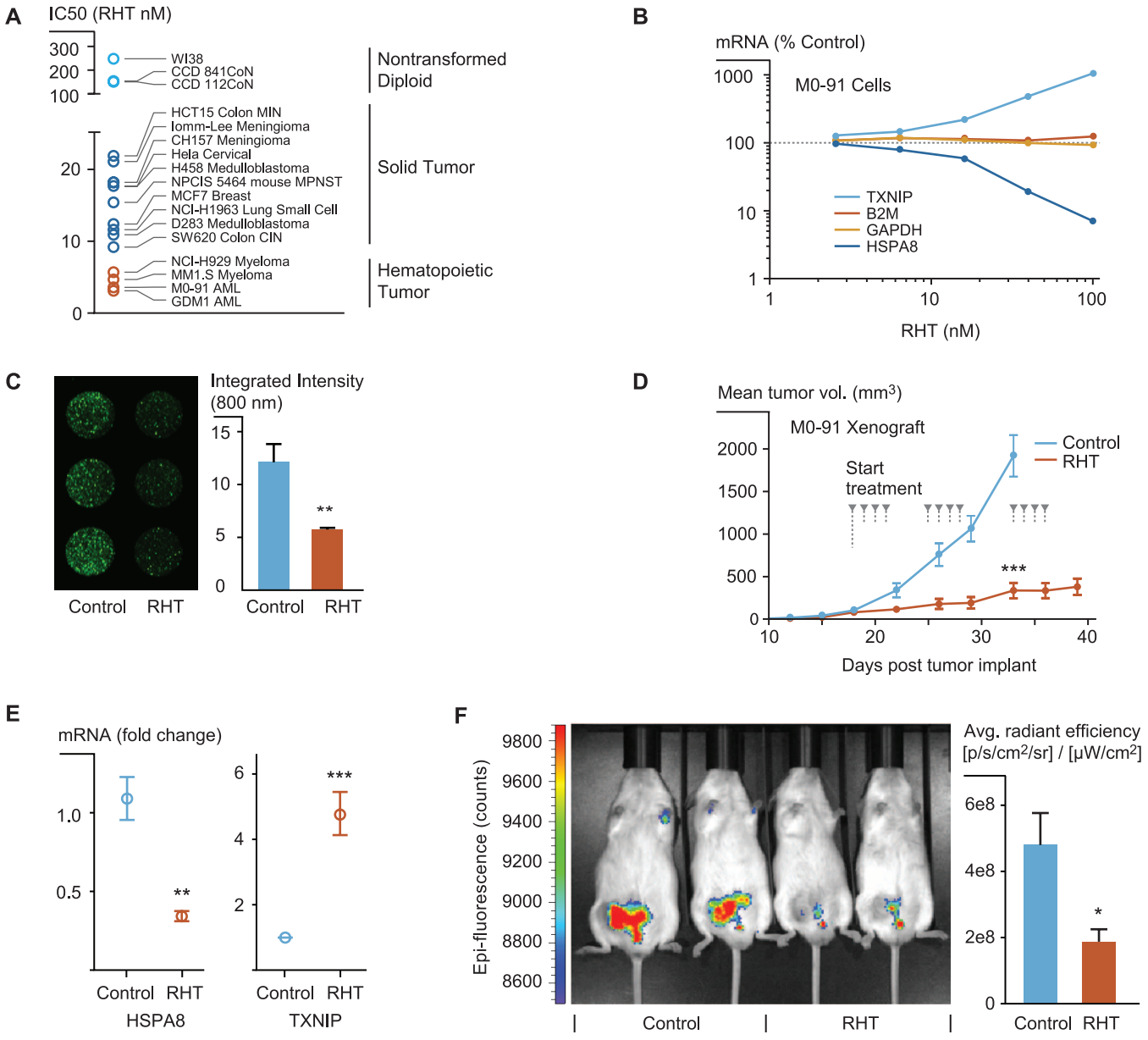

Fig. 7. Rocaglates suppress tumor growth, *HSPA8* mRNA levels and glucose uptake in vivo. (**A**) Scatter plot of IC_{50} values of the growth of a diverse panel of cell lines treated with RHT. Cells were treated for 5 days. Red indicates hematopoietic cancer lines, dark blue indicates solid tumor cell lines, and light blue indicates euploid nontransformed cells. (**B**) mRNA levels of *HSPA8*, *TXNIP*, and control housekeeping genes in M0-91 cells treated with RHT. Mean of duplicates are reported. (**C**) Glucose uptake of of IR Dye 800CW 2-deoyglucose (2-DG) in M0-91 cell lines treated with RHT. Imaging was performed by using LICOR. (Right) Quantitation of measured intensity (error bars indicate mean ± SEM; $P < 0.005$, two-tailed *t* test, $n = 4$ replicates). (**D**) Plot of the tumor volume of M0-91 acute myeloid leukemia xenografts treated with vehicle or RHT. The mean tumor volume (in cubic millimeters) is plotted over time. Mice were treated with subcutaneous injections starting on day 18 after implantation [either vehicle alone or RHT (1 mg/kg), on days marked by downward pointing arrows]. Eight mice were in each treatment group (error bars indicate mean ± SEM; $P < 0.0001$). (**E**) RT-PCR analysis of HSPA8 and TXNIP mRNA levels from tumor xenografts after a single treatment of either vehicle or RHT (1 mg/kg, subcutaneous; five mice in each group). Tumors were harvested 4 hours after treatment (error bars indicate mean ± SEM; HSPA8, $P < 0.005$; TXNIP, $P < 0.0005$, two-tailed *t* test, $n = 5$ replicates). (**F**) Representative image of epifluorescence of IRDye 800CW 2-deoxyglucose (2-DG) uptake in M0-91 xenografts. Mice bearing tumors were treated with vehicle or RHT (1 mg/kg) as described in the supplementary materials, materials and methods; four mice in each group. Images were acquired 48 hours after the last treatment. (Right) Quantitation of measured radiant efficiency from epifluorescence of IRDye 800CW 2-DG from images of M0-91 xenografts (error bars indicate mean ± SEM; $P = 0.031$, two-tailed *t* test, $n = 4$ replicates).

LINCS Analysis

To identify chemical and genetic modulators that are correlated with HSF1 inactivation, we queried LINCS supported by the NIH Common Fund. This resource at the Broad Institute is a massive expression-profiling initiative to catalog the cellular consequences of both small-molecule and genetic perturbations. The expression data were generated by using a high-throughput Luminex-based assay (Luminex, Austin, TX) as described previously (*43*). Whole-genome expression profiles are inferred from changes in the expression of 1000 landmark genes. The changes in gene expression resulting from each of the genetic and chemical perturbations are rank-ordered from highest to lowest according to their differential expression relative to control treatments. Changes in gene expression caused by a novel perturbation (the "query" signature) can then be compared with the cataloged expression profiles. Profiles that are positively correlated with the query signature are given a positive score, whereas profiles that are negatively correlated to the query signature are given a negative score.

For the analysis, we generated an HSF1 inactivation signature (table S4) of the 50 genes most positively regulated (reduced expression upon HSF1 depletion with shRNA) and 10 genes most negatively regulated (increased expression upon HSF1 depletion with shRNA) in the breast cancer cell lines, MCF7 and BPLER (*44*) [average of the difference between the ha6 shRNA and scrambled shRNA control values between the two cell lines (*8*)], that were also bound by HSF1 in our ChIP-seq experiments. This signature was used to query all 161,636 shRNA and compound signatures (collapsed from a total of 614,216 individual profiles from at least three biological replicates) in the LINCS data set produced in nine cell lines (MCF7, breast cancer; HT29, colon cancer; HEPG2, hepatoblastoma; A549, lung cancer; HCC515, lung cancer; A375, melanoma; PC3, prostate cancer; VCAP, prostate cancer; HA1E, immortalized but nontransformed kidney epithelium). A connectivity score was assigned to each of the expression profiles from the 161,636 perturbations on the basis of a weighted Kolmogorov-Smirnov statistic as previously described (*42*, *43*). GSEA (*42*) was performed on this rank-ordered list in order to determine gene or chemical classes that were most enriched among the positively and negatively connected signatures. The sets analyzed by means of GSEA encompassed the shRNAs corresponding to the genes comprising all 186 KEGG pathway gene sets. The sets also included 110 chemical classes grouped according to the Anatomical Therapeutic Chemical (ATC) Classification System. In addition, we added a set composed of elongation initiation factors. Statistical significance was tested by using 100 random sets size-matched to the set being tested.

Reporter cell lines

Y9 reporter NIH3T3 cells (*45*) were infected with lentivirus for the doxycycline regulatable pTRIPZ-nonsilencing construct (RHS4743). These cells were heat shocked and incubated with doxycycline and then sorted by use of flow cytometry to isolate strong enhanced GFP (eGFP) and Turbo RFP (tRFP) expressors. Sorting was repeated twice for enrichment. Noninduced cells were sorted to remove cells expressing eGFP and tRFP at baseline to make R4.1.B4 cells.

To make the high-throughput screening cell line NIH3T3HGL, the parent vector LV-eGFPfLUC was modified by removing the cytomegalovirus promoter and introducing a 470-bp fragment of the human HSP70B′ construct upstream of the eGFP promoter. NIH3T3 cells were infected with lentivirus generated from this construct, and the high eGFP expressors were isolated by means of flow cytometry after heat shock.

High-Throughput Small-Molecule Screen

Described in supplementary materials, materials and methods.

Dual Reporter Cell Assay

Described in supplementary materials, materials and methods.

Rocaglamide/Rocaglate Derivatives

Rocaglamide/rocaglate derivatives were prepared with total synthesis methods as previously described (*12*, *13*).

Nanostring/nCounter Analysis

The cells were lysed at a concentration of 10,000 cells/μL with RTL buffer [Qiagen (Valencia, CA) catalog no. 79216] and dissociated using a cell shredder (Qiagen catalog no. 79656). The total RNA in 5 μl of lysate was hybridized with the capture and reporter probes overnight at 65°C and processed according to the nCounter recommended protocol. Target/probe complexes were immobilized in nCounter Cartridges for data collection using an nCounter Digital. The data was analyzed according to the manufacture's guidelines. All data were normalized to the expression levels of house keeping genes (*ACTB*, *B2M*, *GAPDH*, *GUSB*, *HPRT1*, and *RPL10*).

S35 Labeling

MCF7 cells were grown to confluence in six-well dishes in standard Dulbecco's minimum essential medium (DMEM) (+10% fetal bovine serum). The cells were rinsed twice in 1× phosphate-buffered saline (PBS) and then placed in DMEM without methionine or cysteine [Life Technologies (Guilford, CT) no. 21013024] for 30 min. EasyTag S35 protein labeling mix (NEG772002MC) was added for 15 min. The cells were rinsed twice in 1X PBS and then lysed in TNEK buffer. Cell lysates were prepared in TNEK buffer {50 mM Tris, pH 7.4; NP-40 1%; EDTA 2 mM; KCl 200 mM and protease inhibitor cocktail [Roche Diagnostics (Indianapolis, IN) catalog no. 11836153001]}. Samples (15 μg total protein/lane) were analyzed by means of SDS–polyacrylamide gel electrophoresis. The gel was incubated for 10 min in 0.7 M sodium salicylate and 10% glycerol. The dried gel was used to expose film. Counts per minute were assessed by using a scintillation counter.

Glucose Uptake

500,000 cells plated in 24-well tissue culture plates were treated for 8 hours with RHT. The cells were then washed in 1× PBS (×2) and placed in glucose-free and serum-free DMEM for 20 min. Glucose uptake was measured by using ^{3}H-2-Deoxyglucose (^{3}H-2DG), incubation for 15 min (final 1 μCi/ml, 50 μM 2DG). The cells were washed with 1 ml of cold 1× PBS (×2), lysed with 0.2 M sodium hydroxide, and then counted by use of scintillation. Experiments were performed in triplicate. Parallel treated cultures cells were stained with Sytox-green (Invitrogen, catalog no. S7020) for normalization. Each analysis was performed three times. The SEM is displayed.

Glucose uptake was also measured by using IRD800 2-deoxyglucose (Fig. 7C). M0-91 cells were washed and resuspended in glucose-free medium (10^{6} cells/ml). Cells were dispensed (100 μL/well) in triplicate wells and incubated for 20 min with 5 μM of the IRDye 800CW 2-DG Optical Probe [LI-COR Biosciences (Lincoln, NB) catalog no. 926-08946]. The cells were then washed ×4 with cold PBS, and the signal was acquired by using an infrared Odyssey imaging system (LI-COR Biosciences).

Lactate Production

500,000 cells were plated in 24-well tissue culture plates and were treated for 8 hours. with RHT. After two washes with 1× PBS, the cells were incubated for 30 min at 37°C in 500 μl of filter sterilized 1× Krebs buffer (126 mM NaCl, 2.5 mM KCl, 1.2 mM NaH2PO4, 1.2 mM MgCl2, 2.5 mM CaCl2, 10 mM Glucose, 25 mM NaHCO3, 10 mM HEPES-KOH pH 7.4). The supernatant was collected, and the lactate was measured with a Lactate Assay Kit [BioVision (Milpitas, CA) catalog no. K-607) according to the manufacturer's guidelines. Parallel treated cultures cells were stained with Sytox Green (Invitrogen, catalog no. S7020) for normalization. Each analysis was performed three times. The SEM is displayed.

Cell Viability Assay

Relative cell growth and survival were measured in 96-well microplate format by using the fluorescent detection of resazurin dye reduction as an endpoint (544 nm excitation and 590 nm emission). Two thousand adherent cells and 10,000 suspension cells were plated 24 hours before compound exposure (for 72 hours). Each analysis was performed three times. For all bar graphs, the SEM is displayed, unless indicated otherwise.

Immunohistochemistry

Paraffin blocks of human colon adenocarcinoma tissue were obtained from the archives of BWH in accordance with the regulations for excess tissue use stipulated by the BWH institutional review

board. Immunohistochemistry for HSF1 was performed as previously described (*8*).

Drug Metabolism and Pharmacokinetic Studies

Described in supplementary materials, materials and methods.

Xenograft Experiment

5e7 M0-91 cells were implanted with Matrigel (BD Biosciences, San Jose, CA) subcutaneously in the right inguinal region of NOD-SCID mice. When the mean tumor volume reached 100 mm^3, RHT formulated in hydroxypropyl beta-cyclodextrin was administered by means of subcutaneous parenteral administration (1 mg/kg) according to the treatment schedule shown in Fig. 7D. Tumor size was measured twice each week by a lab member (M.D.) who was blinded to the treatment groups. There were eight mice in each treatment group (RHT-treated or vehicle-treated). Body weight was measured twice each week. Body condition score (BCS) as monitored by facility vets did not go below 2+ in either treatment group throughout the experiment.

In Vivo Glucose Uptake Experiment

M0-91 cells were inoculated into the inguinal region of NOD-SCID mice. Seventeen days later, the mice were treated with a dose of RHT (1 mg/kg; 4 mice) or vehicle control (4 mice). Four hours later, the mice were given retro-orbital injections of 100 µl IRDye 800CW 2-DG Optical Probe (10 nmol; LI-COR Biosciences, no. 926-08946), and then an additional 4 hours later, these mice were again treated with RHT (1mg/kg) or vehicle control. Thirty-six hours after the last RHT dose, mice were imaged (IVIS; excitation 745 nm, emission 800 nm). Data were analyzed by using Living Image software (PerkinElmer, Waltham, MA).

Real-Time PCR

RNA was purified with RNEasy columns (Qiagen, catalog no. 74104). Quantitative PCR to evaluate mRNA levels was performed by using RT2 SYBR Green qPCR Mastermix (SABiosciences) and primer assay pairs (SABiosciences, Valencia, CA) on a 7900HT ABI Detection System.

References and Notes

1. D. Ruggero, P. P. Pandolfi, *Nat. Rev. Cancer* **3**, 179–192 (2003). doi: 10.1038/nrc1015; pmid: 12612653
2. J. C. Chan *et al.*, *Sci. Signal.* **4**, ra56 (2011). doi: 10.1126/scisignal.2001754; pmid: 21878679
3. R. J. White, *Nat. Rev. Mol. Cell Biol.* **6**, 69–78 (2005). doi: 10.1038/nrm1551; pmid: 15688068
4. K. M. Hannan *et al.*, *Mol. Cell. Biol.* **23**, 8862–8877 (2003). doi: 10.1128/MCB.23.23.8862-8877.2003; pmid: 14612424
5. D. Silvera, S. C. Formenti, R. J. Schneider, *Nat. Rev. Cancer* **10**, 254–266 (2010). doi: 10.1038/nrc2824; pmid: 20332778
6. P. P. Roux, I. Topisirovic, *Cold Spring Harb. Perspect. Biol.* **4**, a012252 (2012). doi: 10.1101/cshperspect.a012252; pmid: 22888049
7. F. U. Hartl, M. Hayer-Hartl, *Science* **295**, 1852–1858 (2002). doi: 10.1126/science.1068408; pmid: 11884745
8. M. L. Mendillo *et al.*, *Cell* **150**, 549–562 (2012). doi: 10.1016/j.cell.2012.06.031; pmid: 22863008
9. L. Whitesell, S. Lindquist, *Expert Opin. Ther. Targets* **13**, 469–478 (2009). doi: 10.1517/14728220902832697; pmid: 19335068
10. M. E. Bordeleau *et al.*, *J. Clin. Invest.* **118**, 2651–2660 (2008). pmid: 18551192
11. J. M. Chambers *et al.*, *Org. Lett.* **15**, 1406–1409 (2013). doi: 10.1021/ol400401d; pmid: 23461621
12. C. M. Rodrigo, R. Cencic, S. P. Roche, J. Pelletier, J. A. Porco Jr., *J. Med. Chem.* **55**, 558–562 (2012). doi: 10.1021/jm201263k; pmid: 22128783
13. S. P. Roche, R. Cencic, J. Pelletier, J. A. Porco Jr., *Angew. Chem. Int. Ed. Engl.* **49**, 6533–6538 (2010). doi: 10.1002/anie.201003212; pmid: 20687060
14. X. Jin, D. Moskophidis, N. F. Mivechi, *Cell Metab.* **14**, 91–103 (2011). doi: 10.1016/j.cmet.2011.03.025; pmid: 21723507
15. C. Dai, L. Whitesell, A. B. Rogers, S. Lindquist, *Cell* **130**, 1005–1018 (2007). doi: 10.1016/j.cell.2007.07.020; pmid: 17889646
16. H. Parikh *et al.*, *PLoS Med.* **4**, e158 (2007). doi: 10.1371/journal.pmed.0040158; pmid: 17472435
17. C. A. Stoltzman *et al.*, *Proc. Natl. Acad. Sci. U.S.A.* **105**, 6912–6917 (2008). doi: 10.1073/pnas.0712199105; pmid: 18458340
18. S. Y. Kim, H. W. Suh, J. W. Chung, S. R. Yoon, I. Choi, *Cell. Mol. Immunol.* **4**, 345–351 (2007). pmid: 17976314
19. C. Dai *et al.*, *J. Clin. Invest.* **122**, 3742–3754 (2012). doi: 10.1172/JCI62727; pmid: 22945628
20. Y. C. Tang, B. R. Williams, J. J. Siegel, A. Amon, *Cell* **144**, 499–512 (2011). doi: 10.1016/j.cell.2011.01.017; pmid: 21315436
21. B. R. Williams *et al.*, *Science* **322**, 703–709 (2008). doi: 10.1126/science.1160058; pmid: 18974345
22. S. Santagata *et al.*, *Proc. Natl. Acad. Sci. U.S.A.* **108**, 18378–18383 (2011). doi: 10.1073/pnas.1115031108; pmid: 22042860
23. F. Fang, R. Chang, L. Yang, *Cancer* **118**, 1782–1794 (2012). doi: 10.1002/cncr.26482; pmid: 22009757
24. L. Alinari *et al.*, *Clin. Cancer Res.* **18**, 4600–4611 (2012). doi: 10.1158/1078-0432.CCR-12-0839; pmid: 22791882
25. R. Cencic *et al.*, *PLoS ONE* **4**, e5223 (2009). doi: 10.1371/journal.pone.0005223; pmid: 19401772
26. D. M. Lucas *et al.*, *Blood* **113**, 4656–4666 (2009). doi: 10.1182/blood-2008-09-175430; pmid: 19190247
27. M. Okabe *et al.*, *Leuk. Res.* **19**, 933–943 (1995). doi: 10.1016/0145-2126(95)00039-9; pmid: 8632663
28. L. Meng, V. L. Gabai, M. Y. Sherman, *Oncogene* **29**, 5204–5213 (2010). doi: 10.1038/onc.2010.277; pmid: 20622894
29. S. Santagata *et al.*, *ACS Chem. Biol.* **7**, 340–349 (2012). doi: 10.1021/cb200353m; pmid: 22050377
30. K. L. Scott *et al.*, *Cancer Cell* **20**, 92–103 (2011). doi: 10.1016/j.ccr.2011.05.025; pmid: 21741599
31. V. L. Gabai *et al.*, *Mol. Cell. Biol.* **32**, 929–940 (2012). doi: 10.1128/MCB.05921-11; pmid: 22215620
32. S. D. Westerheide, J. Anckar, S. M. Stevens Jr., L. Sistonen, R. I. Morimoto, *Science* **323**, 1063–1066 (2009). doi: 10.1126/science.1165946; pmid: 19229036
33. O. Brandman *et al.*, *Cell* **151**, 1042–1054 (2012). doi: 10.1016/j.cell.2012.10.044; pmid: 23178123
34. J. S. Hahn, Z. Hu, D. J. Thiele, V. R. Iyer, *Mol. Cell. Biol.* **24**, 5249–5256 (2004). doi: 10.1128/MCB.24.12.5249-5256.2004; pmid: 15169889
35. A. L. Hsu, C. T. Murphy, C. Kenyon, *Science* **300**, 1142–1145 (2003). doi: 10.1126/science.1083701; pmid: 12750521
36. S. D. Chou, T. Prince, J. Gong, S. K. Calderwood, *PLoS ONE* **7**, e39679 (2012). doi: 10.1371/journal.pone.0039679; pmid: 22768106
37. S. M. Hensen *et al.*, *Cell Stress Chaperones* **17**, 743–755 (2012). doi: 10.1007/s12192-012-0347-1; pmid: 22797943
38. T. Peng, T. R. Golub, D. M. Sabatini, *Mol. Cell. Biol.* **22**, 5575–5584 (2002). doi: 10.1128/MCB.22.15.5575-5584.2002; pmid: 12101249
39. L. Whitesell, S. Santagata, N. U. Lin, *Curr. Mol. Med.* **12**, 1108–1124 (2012). doi: 10.2174/156652412803306657; pmid: 22804235
40. N. L. Solimini, J. Luo, S. J. Elledge, *Cell* **130**, 986–988 (2007). doi: 10.1016/j.cell.2007.09.007; pmid: 17889643
41. J. Lamb *et al.*, *Science* **313**, 1929–1935 (2006). doi: 10.1126/science.1132939; pmid: 17008526
42. A. Subramanian *et al.*, *Proc. Natl. Acad. Sci. U.S.A.* **102**, 15545–15550 (2005). doi: 10.1073/pnas.0506580102; pmid: 16199517
43. D. Peck *et al.*, *Genome Biol.* **7**, R61 (2006). doi: 10.1186/gb-2006-7-7-r61; pmid: 16859521
44. T. A. Ince *et al.*, *Cancer Cell* **12**, 160–170 (2007). doi: 10.1016/j.ccr.2007.06.013; pmid: 17692807
45. T. J. Turbyville *et al.*, *J. Nat. Prod.* **69**, 178–184 (2006). doi: 10.1021/np058095b; pmid: 16499313

Acknowledgements: We thank T. Volkert, J. Love, S. Gupta, and the WIBR–Genome Technology Core for sequencing support; S. Malstrom (Koch Institute for Integrative Cancer Research) for assistance with in vivo imaging; G. Bell, P. Thiru, and A. Lancaster for assistance with informatics analysis; the Connectivity Map team at the Broad Institute for generation of the LINCS data set and query tools; Joe Negri and the MLPCN team at the Broad Institute for chemical screening; and M. Duquette for assistance with animal experiments. We also thank C. Rodrigo (Boston University) for compound synthesis. We thank the Lindquist laboratory for helpful discussions and suggestions. The work was supported by the Johnson & Johnson's Corporate Office of Science and Technology focused funding program (L.W.), the Marble Fund (S.L.), and NIH R01 CA175744-01 (L.W.). The MLPCN screen was supported by R03 MH086465-01 and R03 DA027713-01 to L.W. This work was supported by the NIH Common Fund's LINCS program (5U54HG006093, "Large scale gene expression analysis of cellular states") to T.R.G. J.A.P. Jr. is supported by R01 GM073855. S.L. is an Investigator of the Howard Hughes Medical Institute. M.L.M. was supported by American Cancer Society New England Division–SpinOdyssey (PF-09-253-01-DMC). S.S. is supported by NIH (K08NS064168), the Brain Science Foundation, the American Brain Tumor Association, the Beez Foundation, the V Foundation, and the Jared Branfman Sunflowers for Life Fund. The expression profiling and ChIP-Seq data are deposited in GEO (GSE45853). The MLPCN chemical screening data are deposited in Pubchem (AID: 2118).

Supplementary Materials

www.sciencemag.org/content/full/341/6143/1238303/suppl/DC1

Materials and Methods
Figs. S1 to S9
Reference (*46*)
Tables S1 to S5

25 March 2013; accepted 24 May 2013
10.1126/science.1238303